

# Microstructures and Elevated Temperature Mechanical Properties of As-extruded ZM61-Sn Alloys

Tang Tian<sup>1,2</sup>, Zhang Dingfei<sup>1,2</sup>, Hu Guangshan<sup>1,2</sup>, Xu Junyao<sup>1,2</sup>, Pan Fusheng<sup>2,3</sup>

<sup>1</sup>College of Materials Science and Engineering, Chongqing University, Chongqing 400045, China; <sup>2</sup>National Engineering Research Center for Magnesium Alloys, Chongqing University, Chongqing 400044, China; <sup>3</sup>Chongqing Academy of Science and Technology, Chongqing 401123, China

**Abstract:** Microstructures, elevated temperature mechanical properties and fracture mechanisms of the as-extruded ZM61- $x$ Sn ( $x=2, 4, 8$ , wt%) alloys were investigated by optical microscope (OM), X-ray diffraction (XRD), scanning electron microscope (SEM) and high temperature tensile tests. The results reveal that the addition of Sn can refine microstructures and the refinement effect increases with the increase of Sn content. The average grain sizes of the as-extruded ZM61- $x$ Sn ( $x=2, 4, 8$ ) alloys are 11, 8 and 4  $\mu\text{m}$ , respectively. With the increasing of Sn amount, the strength of experimental alloys increases at first and decreases afterward. ZM61-4Sn alloy shows the highest strength, whose ultimate tensile strength and yield strength are 216 and 173 MPa tested at 180  $^{\circ}\text{C}$ , respectively. The ductility increases with the content of Sn increasing, and the elongation of as-extruded ZM61- $x$ Sn ( $x=2, 4, 8$ ) alloys are 183.8%, 235.8% and 258.6%, respectively, when tensile temperature reaches 300  $^{\circ}\text{C}$ . The ZM61-4Sn alloy has the optimal coalescence of strength and ductility. The localized necking leads to the final fracture of the specimens and the micro-void coalescence is the main fracture mechanism. Incomplete dynamic recrystallization occurs when tensile tests are carried out at 260 and 300  $^{\circ}\text{C}$ .

**Key words:** ZM61-Sn alloy; extrusion; microstructure; elevated temperature mechanical properties

As the lightest structural metallic materials, magnesium (Mg) alloys exhibit great potential applications in automobile and aerospace for decreasing the mass of vehicles and improving fuel consumption<sup>[1-3]</sup>. However, poor mechanical properties at elevated temperatures restrict their further applications in some high temperature parts (such as engine<sup>[4,5]</sup>). Therefore, the development of new heat resistant Mg alloys with excellent mechanical properties is essential. Previous investigations have revealed that alloying is an effective method to improve the elevated temperature mechanical properties of Mg alloys and the rare earth elements (RE) such as Nd, Y, Ce are commonly used<sup>[6-8]</sup>. However, the high cost of rare earth elements restricts their wide applications. It is necessary to develop promising Mg alloys with good elevated temperature mechanical properties and without RE elements.

According to the Mg-Sn binary phase diagram, the maximum solid solubility of Sn is 14.85 wt%, and its eutectoid temperature is 561  $^{\circ}\text{C}$  which is similar to those of some rare earth elements<sup>[9]</sup>. Some studies have reported that the addition of Sn element can effectively refine grains, form high melting, high hardness and good thermally stable Mg<sub>2</sub>Sn intermetallics in Mg alloys<sup>[10,11]</sup>. Consequently, Sn element has a huge potential to replace the RE element to enhance the elevated temperature properties of Mg alloys<sup>[12]</sup>. Chen<sup>[13]</sup> et al have found that the added 0.5 wt% Sn into ZA62 alloys can enhance their heat resistance owing to the fine Mg<sub>2</sub>Sn phase disperse in matrix.

Compared with cast Mg alloys, wrought Mg alloys have better mechanical properties. As a new high strength wrought Mg alloys, ZM61 has a wide application due to its relatively low price. The effects of Sn element on the mi-

Received date: August 20, 2016

Foundation item: National Great Theoretic Research Project (2013CB632200); National Natural Science Foundation of China (51474043); Chongqing Municipal Government Project (CSTC2013JCYJC60001); Education Commission of Chongqing Municipality (KJZH14101); Sharing Fund of Chongqing University's Large-scale Equipment

Corresponding author: Zhang Dingfei, Ph. D., Professor, College of Materials Science and Engineering, Chongqing University, Chongqing 400045, P. R. China, Tel: 0086-23-65112491, E-mail: zhangdingfei@cqu.edu.cn

Copyright © 2017, Northwest Institute for Nonferrous Metal Research. Published by Elsevier BV. All rights reserved.

microstructure and room temperature strength in ZM61 have been investigated, but its elevated temperature performance is not involved. In the present paper, Sn element was added into the ZM61 Mg alloy for high-temperature tensile experiments, to investigate the microstructures and elevated temperature mechanical properties of the as-extruded Mg-Zn-Mn-Sn alloys.

## 1 Experiment

Commercial high purity Mg (>99.9%), Zn (>99.9%), Sn (>99.9%) and Mg-4.1Mn (wt%) master alloys were used to prepare the experimental alloys. These alloys were heated to about 720 °C in an electrical resistance furnace under Ar protecting atmosphere. The chemical composition of the experimental alloys is listed in Table 1. Then the castings were homogenized at 330 °C for 15 h and 420 °C for 2 h directly followed by water quenching. The homogenized alloys were extruded to bars of 16 mm in diameter at 350 °C with the extrusion rate of 1~2 m/min and extrusion ratio of 25. The extruded bars were machined to be tensile test specimens with 25 mm in gauge length and 5 mm in diameter. The tensile tests were carried out in CMT-5105 stretcher at a speed of 3mm/min at four different temperatures (180, 220, 260 and 300 °C). The specimens were first heated to the deformation temperature at the rate of 20 °C/min, and then held for 8 min to guarantee isothermally. The tensile directions were parallel to the extrusion direction. In each condition three specimens were used to ensure the data's reproducibility.

The chemical composition was analyzed by a XRF-1800 CCDE sequential X-ray fluorescence spectrometer. Phase components were characterized by a Rigaku D/max 2500 PC X-ray diffractometer using Cu-K $\alpha$ . The optical microstructures of specimens were photographed by a LEXT 2000 laser metallographic microscope. The specimens for microstructure observation were ground and etched by acetic-picric etchant (7 mL ethanol, 1 mL acetic acid and 5 g picric acid). Fractured surface morphologies were observed by TESCAN VEGA II scanning electron microscope equipped with an INCA Energy 350 energy dispersive X-ray spectrometer (EDS).

## 2 Results and Discussion

### 2.1 Microstructures of as-extruded ZM61-Sn alloys

Fig.1 shows the XRD patterns of as-extruded ZM61 and ZM61-xSn (x=2, 4, 8, wt%) alloys. Besides  $\alpha$ -Mg matrix, four kinds of second phase are detected in the ZM61-Sn

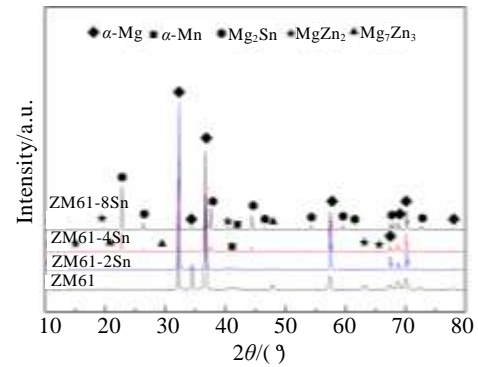


Fig.1 XRD patterns of as-extruded ZM61 and ZM61-xSn alloys

alloys. With the addition of Sn element, a new Mg<sub>2</sub>Sn phase forms<sup>[14]</sup>. The phase composition of ZM61-Sn alloys is  $\alpha$ -Mg,  $\alpha$ -Mn, Mg<sub>2</sub>Sn, MgZn<sub>2</sub> and Mg<sub>7</sub>Zn<sub>3</sub> phases.

Fig.2 shows the microstructures in longitudinal extrusion of as-extruded ZM61-xSn alloys. The fine equiaxed grains in the longitudinal direction suggest that dynamic recrystallization (DRX) occurs during extrusion at 350 °C. The dimension of extrusion streamlines which consist of fragmented second phase increases with the Sn content increasing. Some extremely fine grains exist surrounding the extrusion streamlines which indicates that the irregular fragmented compounds restrain the recrystallized grains growth during the hot extrusion process. The grain sizes decrease gradually with the increase of Sn content and the average values measured by linear intercept are 11, 8 and 4  $\mu$ m, respectively.

The SEM images of the experimental alloys are shown in Fig.3. The extrusion streamlines are principally constituted of Mg<sub>2</sub>Sn and Mg-Zn compounds through the EDS analysis (Table 2). A small number of Mg<sub>2</sub>Sn particles can be found in ZM61-2Sn alloy, but the volume fraction remarkably balloons in ZM61-8Sn alloy, and the dimension of Mg<sub>2</sub>Sn particles aggrandizes with the increase of Sn content, because the undissolved Mg<sub>2</sub>Sn phases are squeezed to fragments during the extrusion, and these fragments distribute along with the longitudinally extruded direction in the form of stringers. In addition, some relatively fine particles distribute in the Mg matrix. They are formed by dynamic precipitation during the extrusion process<sup>[15]</sup>.

### 2.2 Mechanical properties at elevated temperatures

Fig.4 shows the engineering stress and strain curves of the specimens at different tensile temperatures. The engineering stress and strain curves can be divided into four stages, elastic deformation, plastic deformation, localized necking and fracture. The flow stress increases to the peak value first, and then decreases as the strain increases, until to fracture. A rapid decrease in the flow stress can be ob-

Table 1 Chemical composition of ZM61-xSn alloys (wt%)

Alloy	Mg	Zn	Mn	Sn
ZM61-2Sn	91.11	6.15	0.96	1.78
ZM61-4Sn	88.82	6.17	0.85	4.16
ZM61-8Sn	85.13	5.88	0.94	8.05

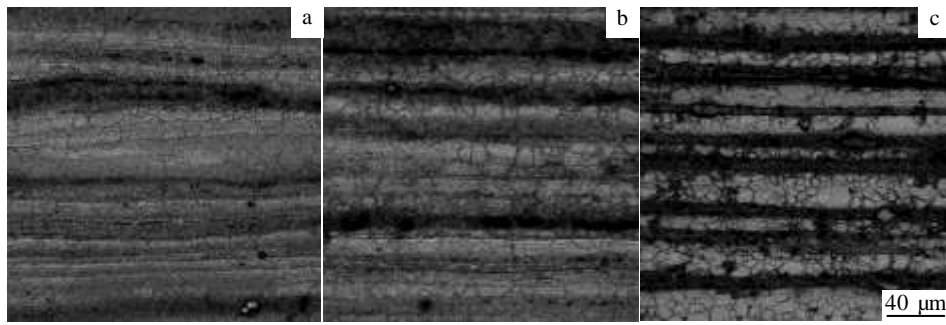


Fig.2 Optical images of ZM61-xSn alloys: (a) ZM61-2Sn, (b) ZM61-4Sn, and (c) ZM61-8Sn

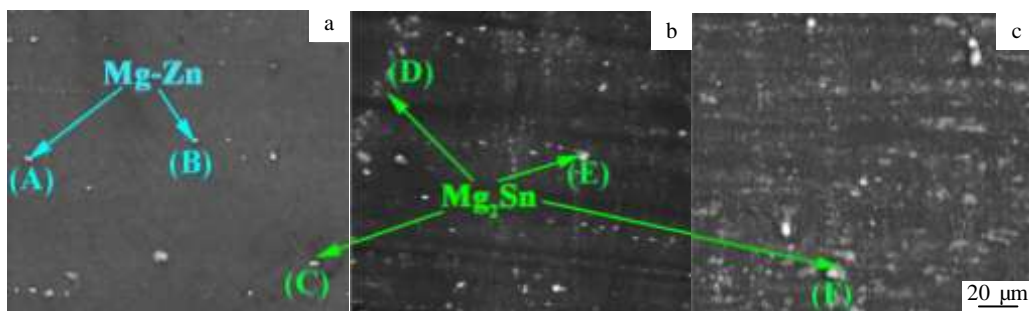


Fig.3 SEM images of ZM61-xSn alloys: (a) ZM61-2Sn, (b) ZM61-4Sn, and (c) ZM61-8Sn

**Table 2 EDS results of the points indicated in Fig.3**

Point	Element/at%			Phase
	Mg	Zn	Sn	
A	35.81	64.19	-	MgZn <sub>2</sub>
B	76.61	23.39	-	Mg <sub>7</sub> Zn <sub>3</sub>
C	64.49	-	35.51	Mg <sub>2</sub> Sn
D	65.24	-	34.76	Mg <sub>2</sub> Sn
E	63.62	-	36.38	Mg <sub>2</sub> Sn
F	67.85	-	32.15	Mg <sub>2</sub> Sn

served when the tensile test were implemented at 180~260 °C, and the rate of decreasing increases with the Sn amounts increase. The stress and strain curves have a steady state in the ZM61-4Sn and ZM61-8Sn alloys when the deformation is at 300 °C. Dislocations multiply remarkably at the beginning of deformation, leading to the work hardening and enhancing the strength of alloy, so the flow stress increases at the initial deformation stage. With the strain increasing dynamic recovery and DRX occur in Mg alloy, leading materials soften, and flow stress gradually declines. Steady state of the stress and strain curves indicates that the work hardening and softening process achieve a dynamical balance<sup>[16,17]</sup>.

Fig.5 shows the tensile properties of the as-extruded ZM61-xSn alloys at different temperatures. The strength and elongation (EL) of alloys are affected by the tension temperature and Sn content. The strength decreases and the

EL increases with the increase of deformation temperature. When tension tests are carried out at 180 °C, the EL of the specimens are 70.7%, 59.5%, 80.9%, and the yield strength (YS) are 158, 173, 147 MPa, respectively. When the deformation temperature reaches to 300 °C, the EL of the specimens are 183.8%, 235.8%, 258.6%, and the YS are 47, 63, 56 MPa, respectively. The dominant deformation mechanisms for Mg alloys at room temperature are the basal slip and twinning. With the temperature increasing, non-basal slip system can be activated. Therefore, the ductility of Mg alloys increases with the deformation temperature increasing<sup>[18]</sup>. The main deformation mechanisms are non-basal dislocation slip and climb at elevated temperature; as a result dynamical recovery and DRX weaken the alloy strength. Therefore, the strength decreases rapidly with the temperature increases.

The strength increases first and then decreases with the increase of Sn. The ZM61-4Sn alloy has the highest ultimate tensile strength (UTS) and YS. The EL increases as the Sn content increases constantly. In conclusion, the alloy with the addition of 4% Sn shows the best coalescence of strength and ductility among the test alloys. The UTS, YS and EL of ZM61-4Sn alloy are 216 MPa, 173 MPa and 59.5% when tensile tested at 180 °C.

The improvement of tensile strength of the experimental alloys can be mainly ascribed to three aspects: (1) the addition of Sn refines the microstructure. According to Hall-

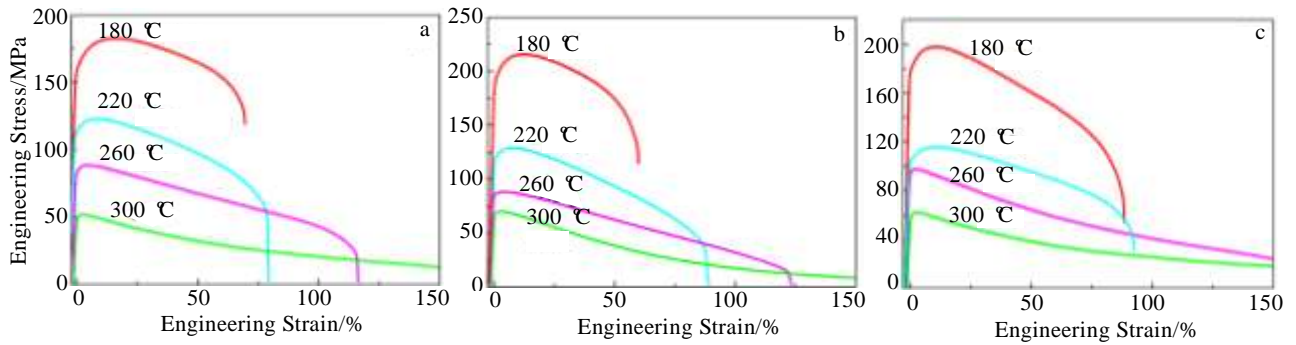


Fig.4 Engineering stress-strain curves of ZM61-*x*Sn alloys tested at different temperatures: (a) ZM61-2Sn, (b) ZM61-4Sn, and (c) ZM61-8Sn

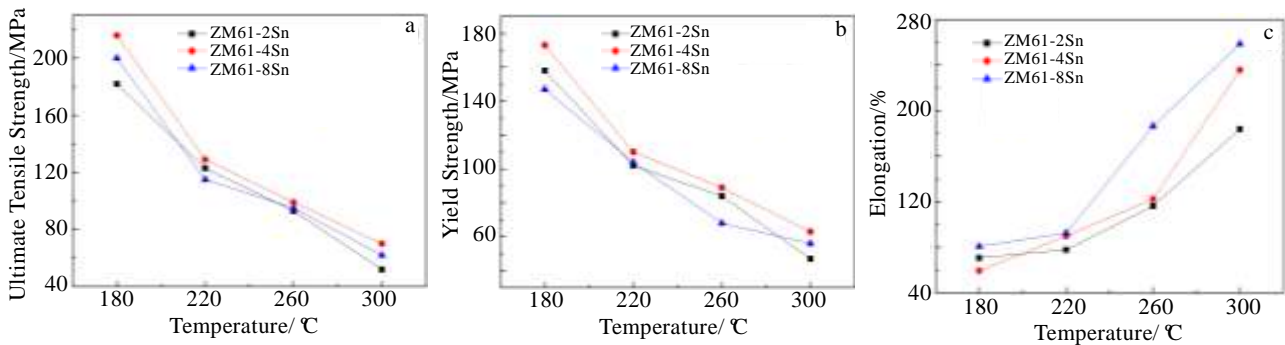


Fig.5 Tensile properties of ZM61-*x*Sn alloys tested at different temperatures: (a) UTS, (b) YS, and (c) EL

Petch relationship ( $\sigma = \sigma_0 + kd^{1/2}$ .  $\sigma$  is yield strength,  $d$  is average grain size,  $\sigma_0$  and  $k$  are constants for the given alloys), the decrease of grain size can greatly enhance the tensile strength of alloys<sup>[19]</sup>. (2) Mg atoms in matrix replaced by Sn and Zn atoms would lead to lattice distortions, hinder the motion of dislocation and improve the strength of the alloys. (3) The discrete  $Mg_2Sn$  particles distributed in grains and boundaries can effectively impede dislocation motion and grain boundary sliding, which increases the strength. However, with the Sn content increasing, the dimension of the  $Mg_2Sn$  phases increases obviously. These coarse  $Mg_2Sn$  phases deteriorate the continuity of Mg matrix, which may act as crack initiation. Therefore, the amount of Sn addition in ZM61 alloys should be limited in a certain range.

### 2.3 Fracture mechanisms

Fig.6 shows the macroscopical image of the fracture specimens tested at different temperatures. The specimens deformation in the gauge segment is quite uniform, and when the deformation temperature is over 260 °C, the specimens exhibit diffuse necking characteristics, which indicates the appearance of DRX<sup>[20]</sup>. An obvious localized necking region can be observed when the deformation are at 260 and 300 °C. The connection strength of the localized necking region can't bear the applied load, leading to the fracture of the specimens.

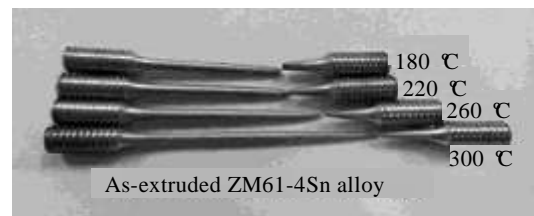


Fig.6 Macroscopical image of the fracture specimens tested at different temperatures

Fig.7 shows the fracture morphologies of ZM61-4Sn alloys tested at different temperatures. In Fig.7a and 7b, the fracture surfaces are composed of a large number of fine dimples. With the tensile temperature increasing, in Fig.7c and 7d, the fracture surfaces are composed of big cavitations, which means micro-void coalescence is the main fracture mechanism. Localized necking is hard to appear at relatively low deformation temperature, so it is likely to form small and shallow dimples. With the increasing of deformation temperature, the material transfer and diffusion ability increase, and these small dimples tend to coalesce to be cavitations<sup>[21]</sup>. The characters of recrystallized grains can also be observed in Fig.7c and 7d.

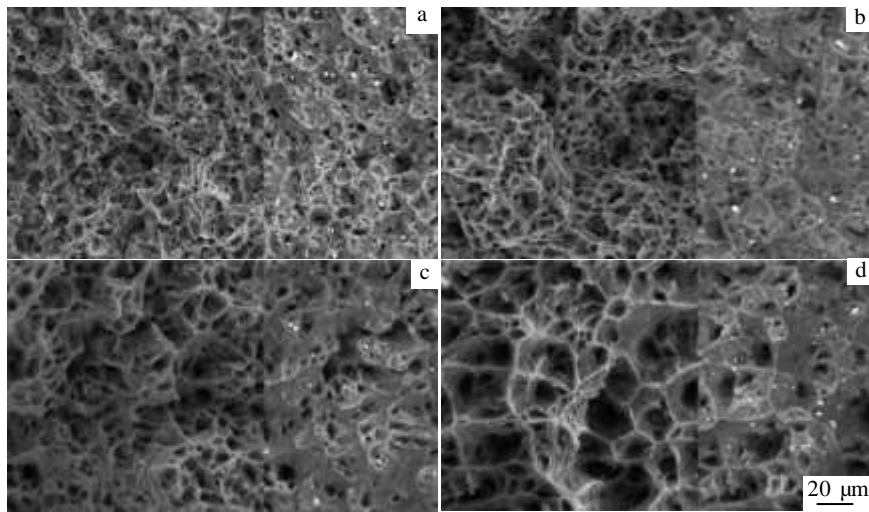


Fig.7 SEM and BSE images of fracture surface of ZM61-4Sn alloys tested at different temperatures: (a) 180 °C, (b) 220 °C, (c) 260 °C, and (d) 300 °C

Fig.8 shows the optical images of the longitudinal section near the fracture surface of the ZM61-4Sn alloys tested at different temperatures. Obviously, the temperature has a significant effect on the microstructures. When the deformation temperature is below 220 °C, the specimens have no obvious transformation compared with the original organization. However, when the tensile temperature reaches 260 °C, the microstructures change inhomogeneous, the fine DRX grains occur in the grain boundaries, as shown in Fig.8c. The volume fraction of DRX grains is increased with the temperature increasing, as shown in Fig.8d.

Mg alloy is a typical material with low stacking fault energy<sup>[22,23]</sup>. The limit of cross slip and climb of edge dislocation is likely to cause DRX in Mg alloys<sup>[24]</sup>. In addition, the

grain boundaries can hinder the motion of dislocation, and a great number of dislocation accumulate around the grain boundaries during the plastic deformation, which promotes the nucleation of DRX at the grain boundaries.

The relatively low deformation temperature can't provide enough energy for the dislocation to free motion, so there is no obvious DRX grains appearing in Fig.8a and 8b. The ability of dislocation movement increases with the increase of temperature, and the dislocation density is higher on account of the high deformation temperature, which would promote the germination of DRX. Consequently, incomplete DRX structures are clearly presented at the deformation temperature of 260 and 300 °C.

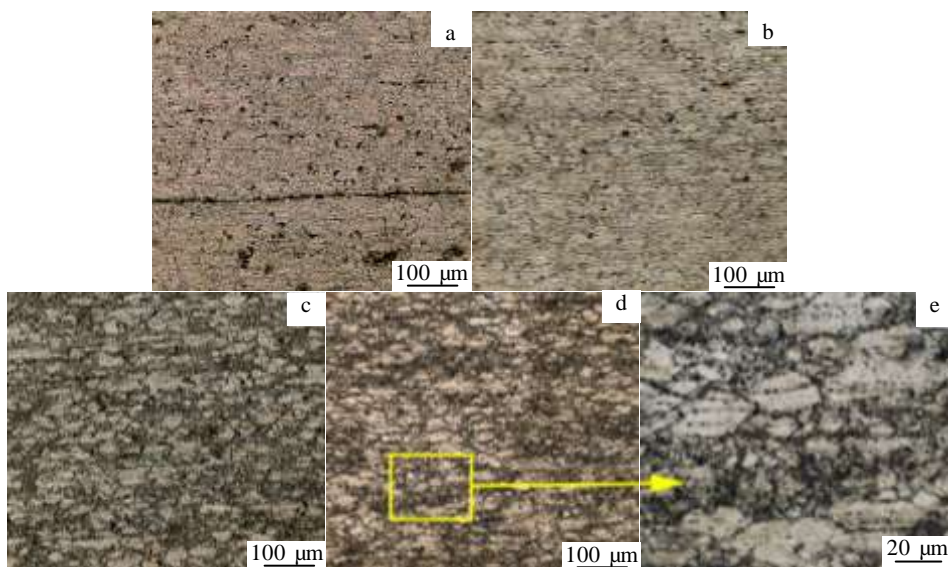


Fig.8 Optical images from longitudinal sections adjacent fracture surface of ZM61-4Sn alloys tested at different temperatures: (a) 180 °C, (b) 220 °C, (c) 260 °C, and (d, e) 300 °C

### 3 Conclusions

1) The phase composition of ZM61- $x$ Sn ( $x=2, 4, 8$ , wt%) alloys is  $\alpha$ -Mg,  $\alpha$ -Mn,  $Mg_7Zn_3$ ,  $Mg_2Sn$  and  $MgZn_2$  phases. The addition of Sn element can remarkably refine the microstructure, and the average grain size are 11, 8 and 4  $\mu\text{m}$ , respectively.

2) The strength increases first and then decreases with the increase of Sn, and the elongation increases constantly with the increase of Sn. The ZM61-4Sn alloy has the optimal coalescence of strength and ductility, and the UTS, YS and EL are 216 MPa, 173 MPa and 59.5%, respectively, when tensile temperature is 180  $^{\circ}\text{C}$ .

3) The localized necking leads to the final fracture of the specimens and the main fracture mechanism is micro-void coalescence. Incomplete DRX occurs when deformation temperature is over than 260  $^{\circ}\text{C}$ .

### References

- 1 Yin D D, Wang Q D, Boehlert C J et al. *Materials Science and Engineering A*[J], 2012, 546: 239
- 2 Chen C J, Wang Q D, Yin D D. *Journal of Alloys and Compounds*[J], 2009, 487(1-2): 560
- 3 Zhang Guanghao, Chen Jihua, Yan Hongge et al. *Journal of Alloys and Compounds*[J], 2014, 592: 250
- 4 Sha G, Li J H, Xu W et al. *Materials Science and Engineering A*[J], 2010, 527(20): 5092
- 5 Zhang Jinghuai, Xu Longjiang, Jiao Yufeng et al. *Materials Science and Engineering A*[J], 2014, 610: 139
- 6 Cheng W L, Park S S, Tang W N et al. *Journal of Rare Earths*[J], 2010, 28(5): 785
- 7 Stefano Spigarelli, Mohamad El Mehtedi. *Scripta Materialia*[J], 2010, 63(7): 704
- 8 Zhang Xiaolong, Wang Zhaohui, Du Wenbo et al. *Materials and Design*[J], 2014, 58: 277
- 9 Kim Y K, Kim Do H, Kim W T et al. *Materials Letters*[J], 2013, 113: 50
- 10 Hasani G H, Mahmudi R. *Materials and Design*[J], 2011, 32(7): 3736
- 11 Dong Xuguang, Fu Junwei, Wang Jing et al. *Materials and Design*[J], 2013, 51: 567
- 12 Ghosh P, Mezbahul-Islam M, Medraj M. *Calphad*[J], 2012, 36: 28
- 13 Chen Jihua, Chen Zhenhua, Yan Hongge et al. *Journal of Alloys and Compounds*[J], 2008, 461(1-2): 209
- 14 Qi Fugang, Zhang Dingfei, Zhang Xiaohua et al. *Journal of Alloys and Compounds*[J], 2014, 585: 656
- 15 Cheng W L, Park S S, You B S et al. *Materials Science and Engineering A*[J], 2010, 527(18-19): 4650
- 16 Wei Shanghai, Zhu Tianping, Michael Hodgson et al. *Materials Science and Engineering A*[J], 2013, 585: 139
- 17 Tang Y Q, Chen Y G, Xiao S F et al. *Rare Metal Materials and Engineering*[J], 2014, 43(6): 1291
- 18 Jäger A, Lukáč P, Gärtnerová V et al. *Journal of Alloys and Compounds*[J], 2004, 378(1-2): 184
- 19 Wang Jianli, Yang Jie, Wu Yaoming et al. *Materials Science and Engineering A*[J], 2008, 472(1-2): 332
- 20 Deng J, Lin Y C, Li S S et al. *Materials and Design*[J], 2013, 49: 209
- 21 Toda Hiroyuki, Shamsudin Zul Azri Bin, Shimizu Kazuyuki et al. *Acta Materialia*[J], 2013, 61(7): 2403
- 22 Zhou M, Lin Y C, Deng J et al. *Materials and Design*[J], 2014, 59: 141
- 23 Lin Y C, Deng J, Jiang Y Q et al. *Materials and Design*[J], 2014, 55: 949
- 24 Shi Baoliang, Luo Tianjiao, Wang Jing et al. *Transactions of Nonferrous Metals Society of China*[J], 2013, 23(9): 2560

## 挤压态 ZM61-Sn 合金的显微组织及高温力学性能

唐 甜<sup>1,2</sup>, 张丁非<sup>1,2</sup>, 胡光山<sup>1,2</sup>, 胥钧耀<sup>1,2</sup>, 潘复生<sup>2,3</sup>

(1. 重庆大学 材料科学与工程学院, 重庆 400045)

(2. 重庆大学 国家镁合金材料工程技术研究中心, 重庆 400044)

(3. 重庆市科学技术研究院, 重庆 401123)

**摘要:** 利用金相显微镜 (OM)、X 射线衍射 (XRD)、扫描电镜 (SEM) 和高温拉伸对挤压态 ZM61- $x$ Sn ( $x=2, 4, 8$ , 质量分数, %) 合金的显微组织、高温力学性能和断裂机制进行了研究。结果表明添加 Sn 元素可有效细化合金组织且细化效果随 Sn 含量的增加而增强。挤压态 ZM61- $x$ Sn ( $x=2, 4, 8$ ) 合金的平均晶粒尺寸分别为 11, 8 和 4  $\mu\text{m}$ 。随 Sn 含量的增加, 合金的力学性能先升高后降低。在所有的实验合金中 ZM61-4Sn 合金的强度最高, 当在 180  $^{\circ}\text{C}$  下进行拉伸实验时, 其极限抗拉强度和屈服强度分别为 216 和 173 MPa。合金的延伸率随 Sn 含量的增加而增加, 当拉伸温度为 300  $^{\circ}\text{C}$  时, ZM61- $x$ Sn ( $x=2, 4, 8$ ) 合金的延伸率分别为 183.8%, 235.8% 和 258.6%。ZM61-4Sn 合金具有最好的强度和塑性的结合。试样最后的断裂主要由局部缩颈引起以及试样的主要断裂机制为显微孔洞聚集。当在 260 和 300  $^{\circ}\text{C}$  下拉伸时, 合金发生了不完全的动态再结晶。

**关键词:** ZM61-Sn 合金; 挤压; 显微组织; 高温力学性能